SUPPORTING INFORMATION

Design and Synthesis of Ir/Ru Pyrochlore Catalysts for the Oxygen Evolution Reaction Based on Their Bulk Thermodynamic Properties

Daniel F. Abbott[a], Rebecca K. Pittkowski[b], Kateřina Macounová[b], Roman Nebel[b], Elena Marelli[a,c], Emiliana Fabbri[a], Ivano E. Castelli[d*],Petr Krtil[b*], Thomas J. Schmidt[a,e*]

[a]*Electrochemistry Laboratory, Paul Scherrer Institut, CH-5232 Villigen PSI, Switzerland*

[b]*J. Heyrovský Institute of Physical Chemistry of the Czech Academy of Sciences, Dolejškova 3, 18223, Prague, Czech Republic*

[c]*Laboratory for Multiscale Materials Experiments, Paul Scherrer Institut, CH-5232 Villigen PSI, Switzerland*

[d]*Department of Energy Conversion and Storage, Technical University of Denmark, DK-2800 Kgs. Lyngby, Denmark*

[e]*Laboratory of Physical Chemistry, ETH Zürich, CH-8093 Zürich, Switzerland*

**Corresponding authors:*

Thomas J. Schmidt (PSI): thomasjustus.schmidt@psi.ch

Petr Krtil (HIPC): petr.krtil@jh-inst.cas.cz

Ivano E. Castelli (DTU): ivca@dtu.dk

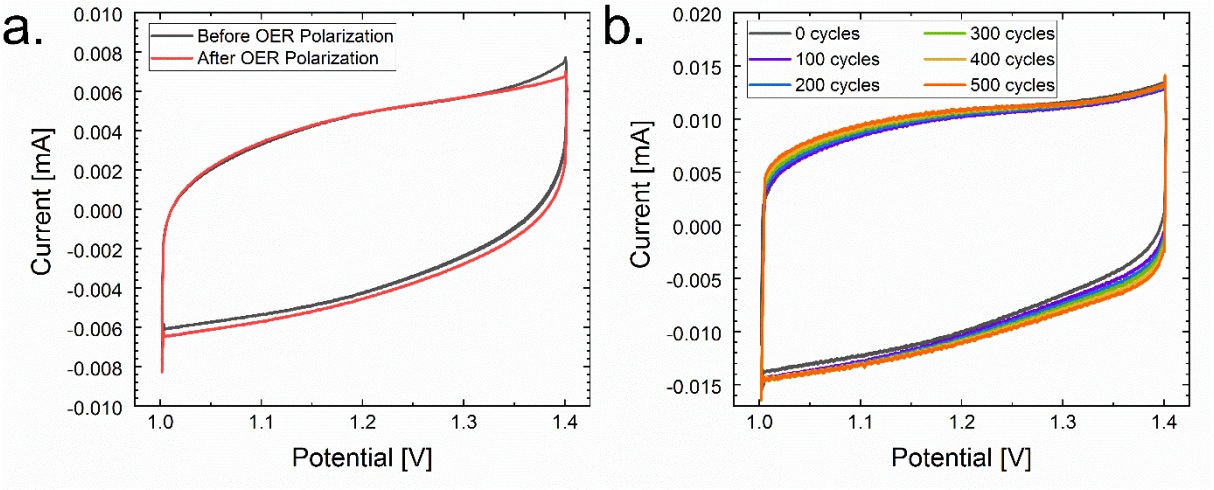

Figure S1. Cyclic Voltammograms of $Gd_2Ir_2O_7$ measured in 0.1 M $HClO_4$ at (a) 10 mV s^{-1} before and after the OER polarization curve measurement, and (b) at 50 mV s^{-1} before the stability protocol (i.e. at 0 cycles) and subsequently after every 100 consecutive potential-step cycles.

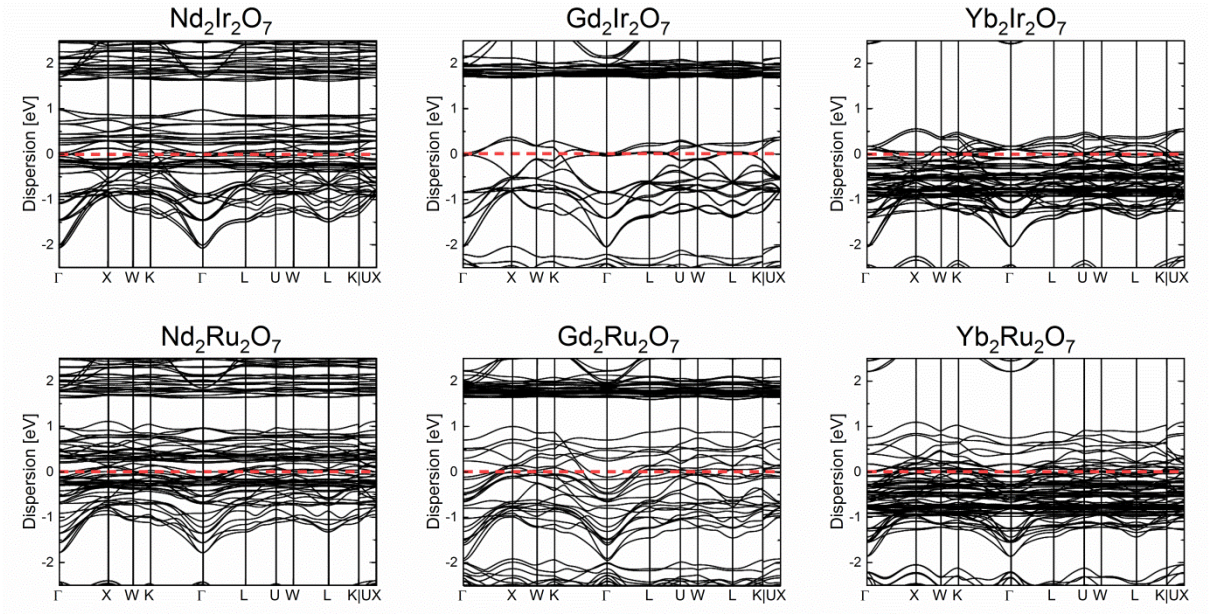

Figure S2. DFT-calculated band structure diagrams for the synthesized rare-earth pyrochlore series. A material is considered to be conductive if the calculated band structure shows bands crossing the Fermi level, which is indicated at 0 eV by the dashed red line.

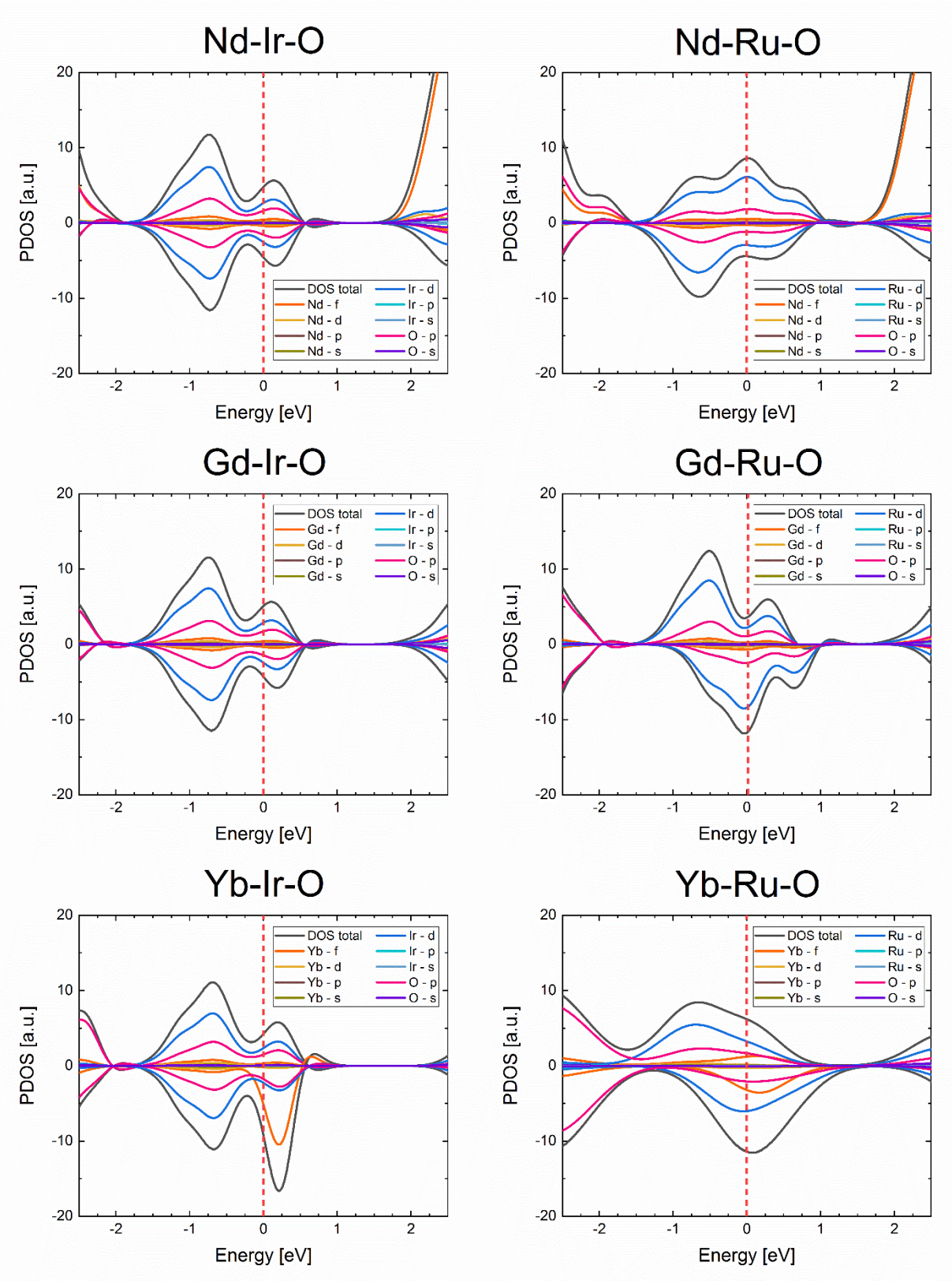

Figure S3. DFT-calculated PDOS diagrams for the synthesized rare-earth pyrochlore series. A material is considered to be conductive if there is no energy gap at the Fermi level, which is indicated at 0 eV by the dashed red line.

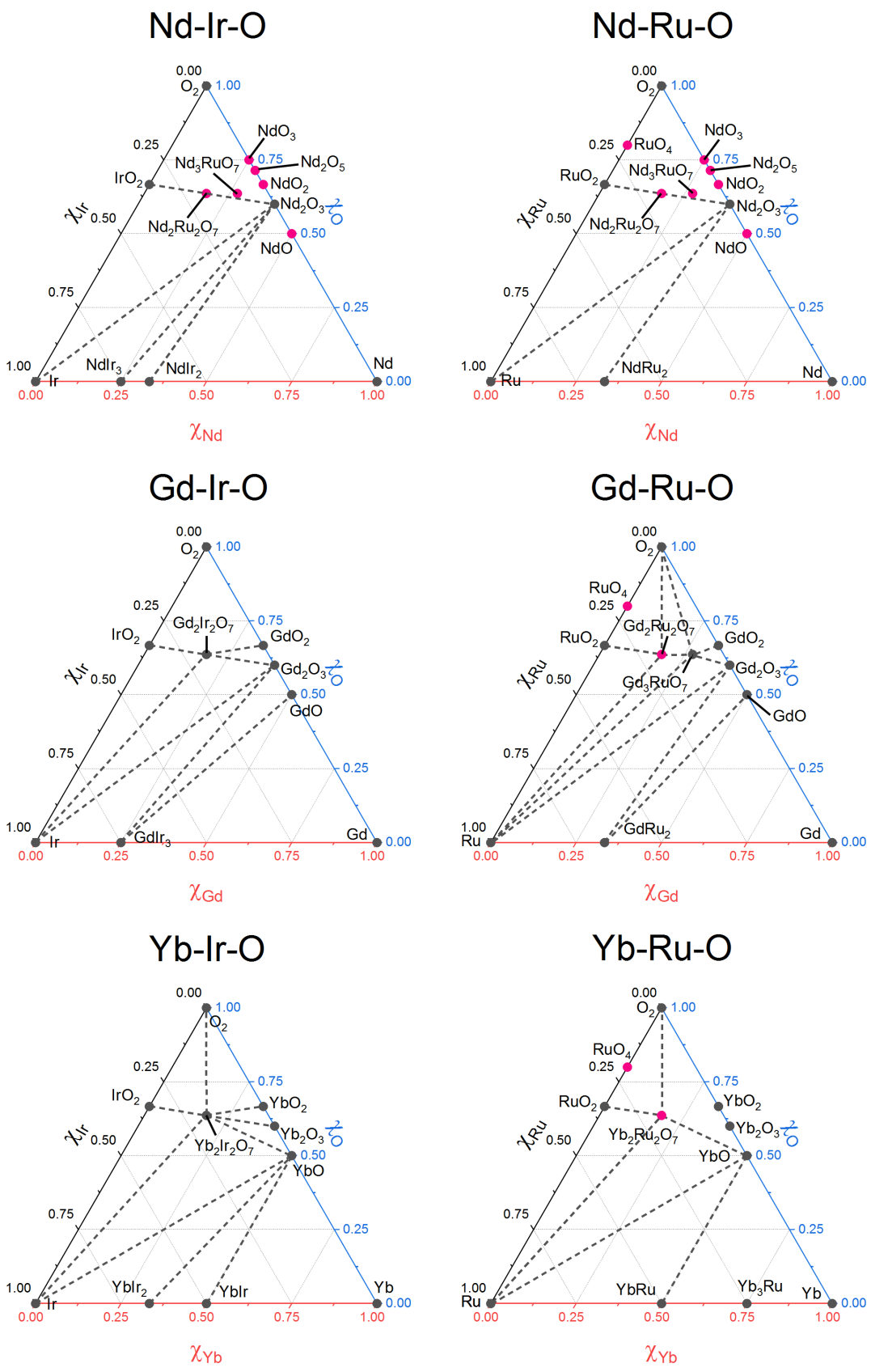

Figure S4. DFT-calculated phase diagrams for the synthesized rare-earth pyrochlore series. Phases that are predicted to be stable are those that appear at the intersection of the convex hulls.

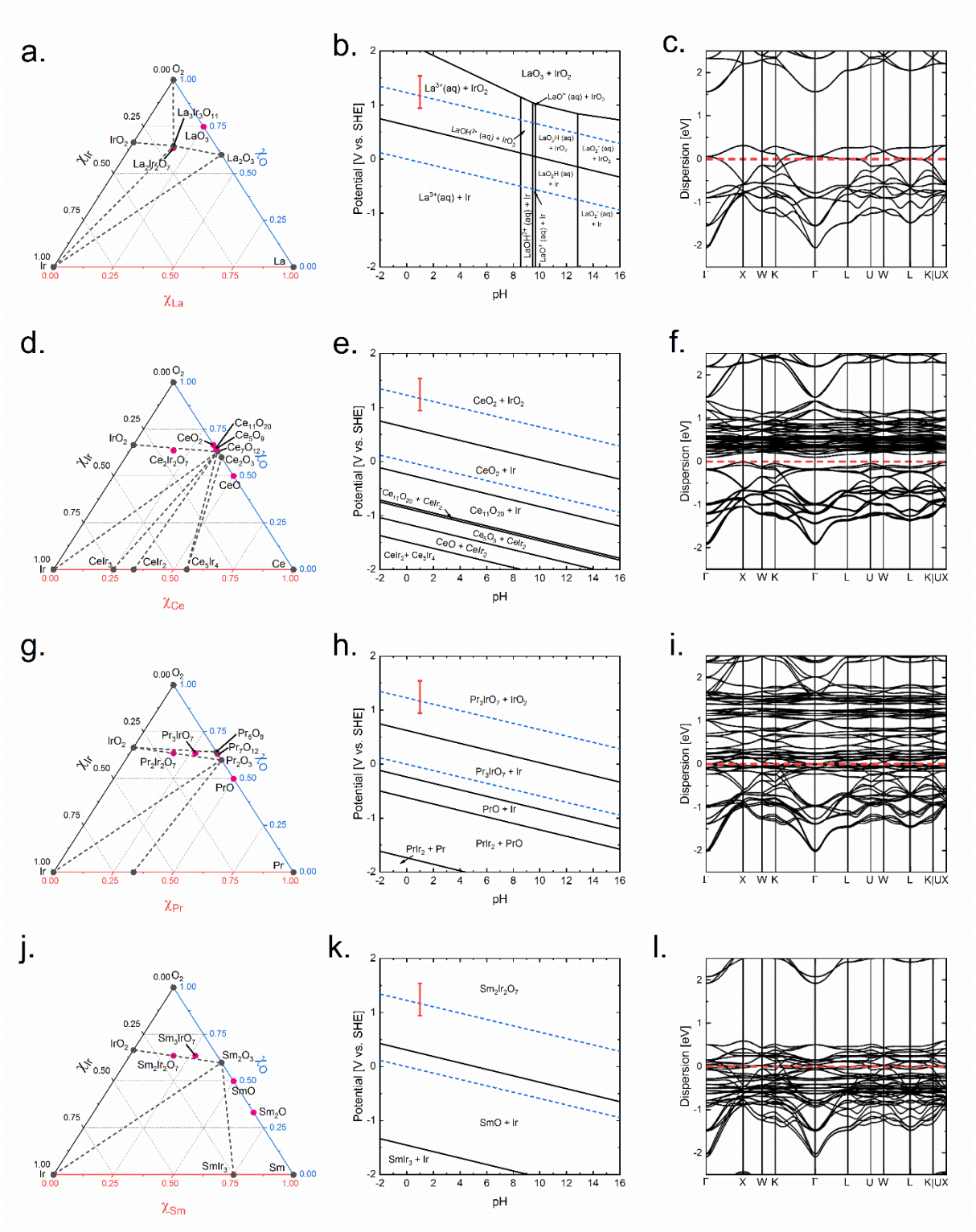

Figure S5. DFT-calculated phase diagrams for the predicted Ir-based rare-earth pyrochlore series. Shown from left to right are the phase diagrams, Pourbaix diagrams, and band energy diagrams for the La-Ir-O (a-c), Ce-Ir-O (d-f), Pr-Ir-O (g-i), and Sm-Ir-O (j-l) systems.

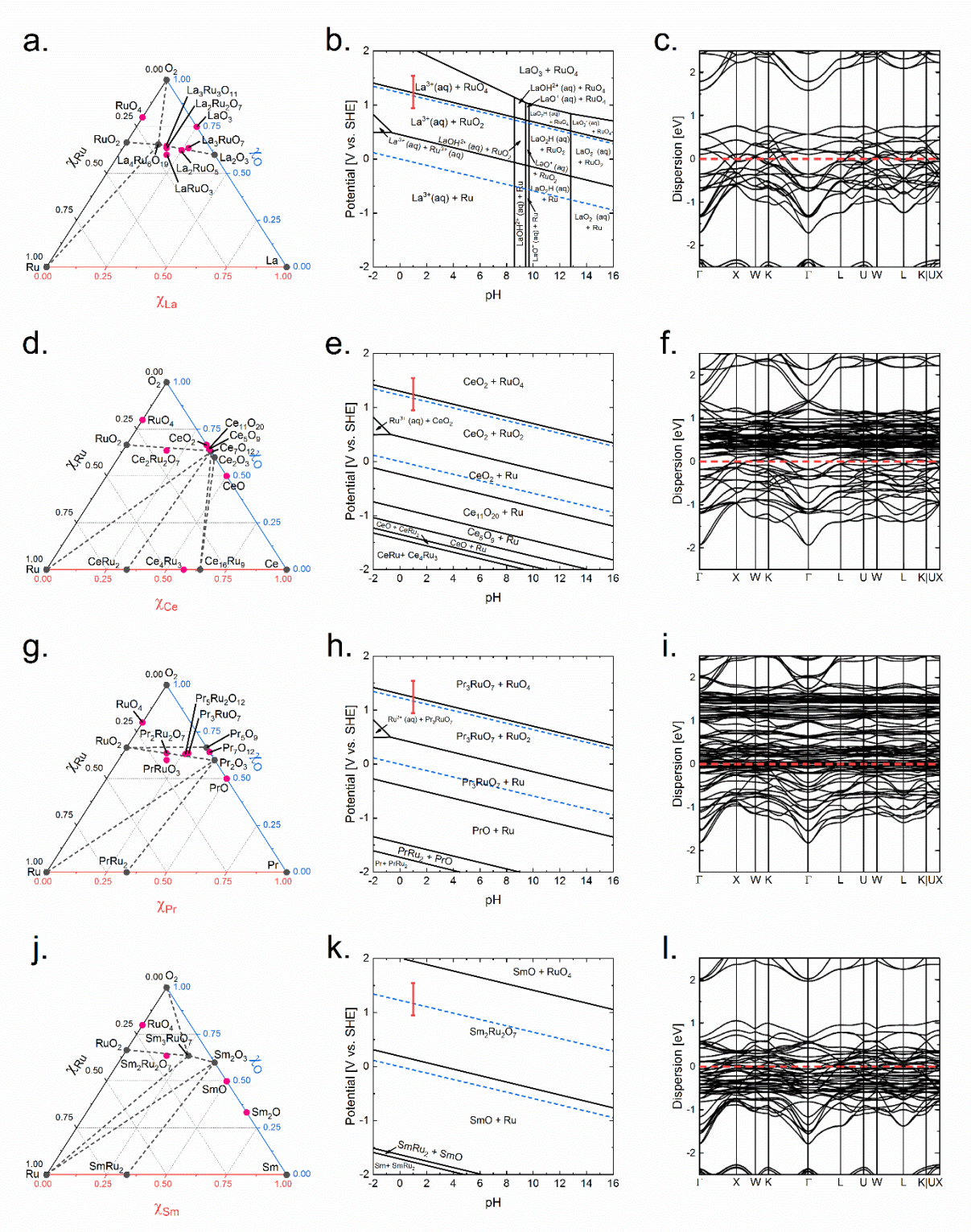

Figure S6. DFT-calculated phase diagrams for the predicted Ru-based rare-earth pyrochlore series. Shown from left to right are the phase diagrams, Pourbaix diagrams, and band energy diagrams for the La-Ru-O (a-c), Ce-Ru-O (d-f), Pr-Ru-O (g-i), and Sm-Ru-O (j-l) systems.

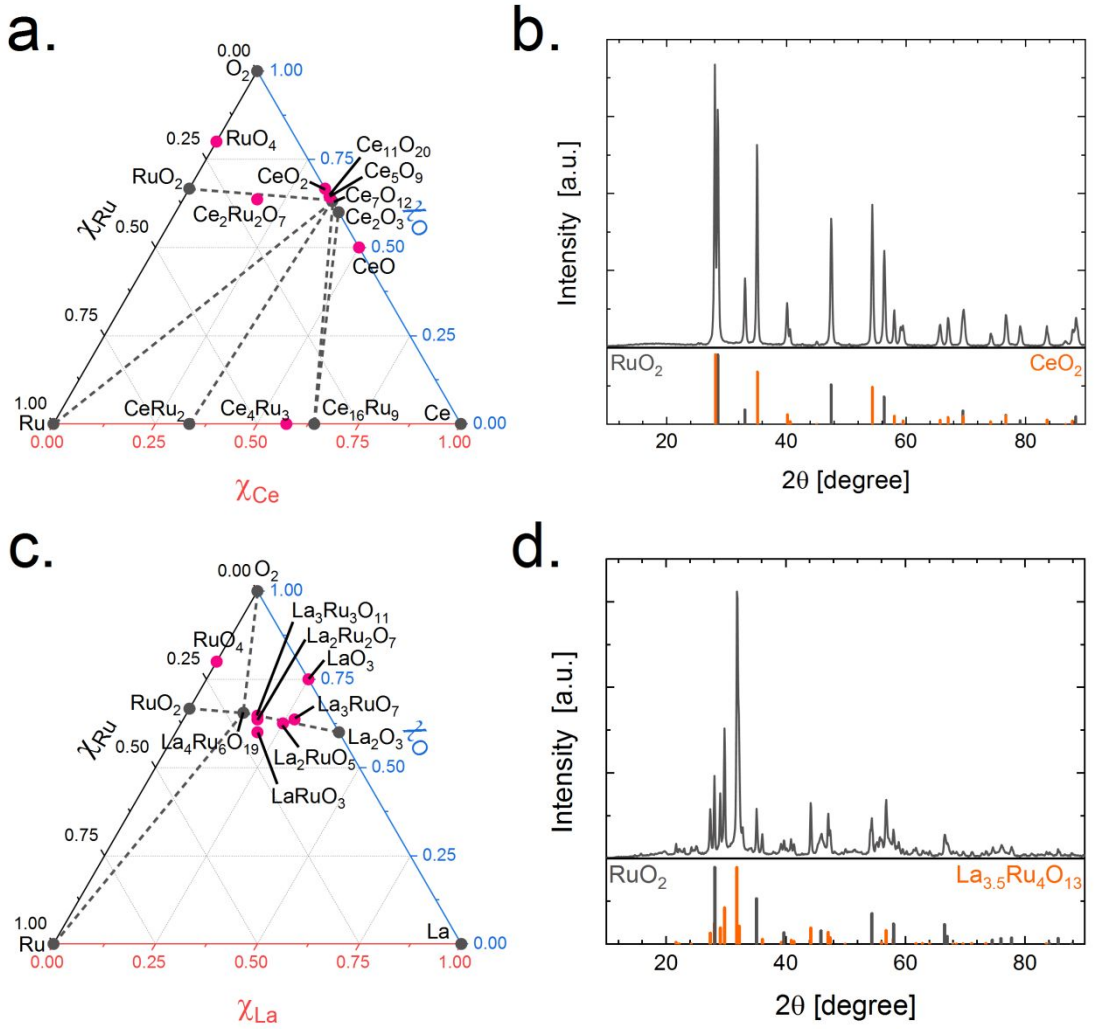

Figure S7. DFT-calculated phase diagrams for the (a) Ce-Ru-O and (b) La-Ru-O systems and the X-ray diffractograms of the obtained powders for the synthesized (c) Ce-Ru-O and (d) La-Ru-O materials.

Table S1. Total energies calculated for the pyrochlore phase ($A_2B_2O_7$) of the screened lanthanide pyrochlore series. Cells shaded in green indicate that the materials are on the convex hull (i.e. stable), while those in orange are metastable (< 0.100 eV/atom) and those in red are predicted to be unstable.

A-site metal	Total energy, eV/atoms	
	B = Ir	B = Ru
La	0.008212343024504	0.018927057178768
Ce	0.153479300925359	0.159339366006448
Pr	0.050538937499865	0.079146666136281
Nd	0.079800935227137	0.076835777499913
Sm	0.144289717045632	0.203447454015159
Gd		
Yb		

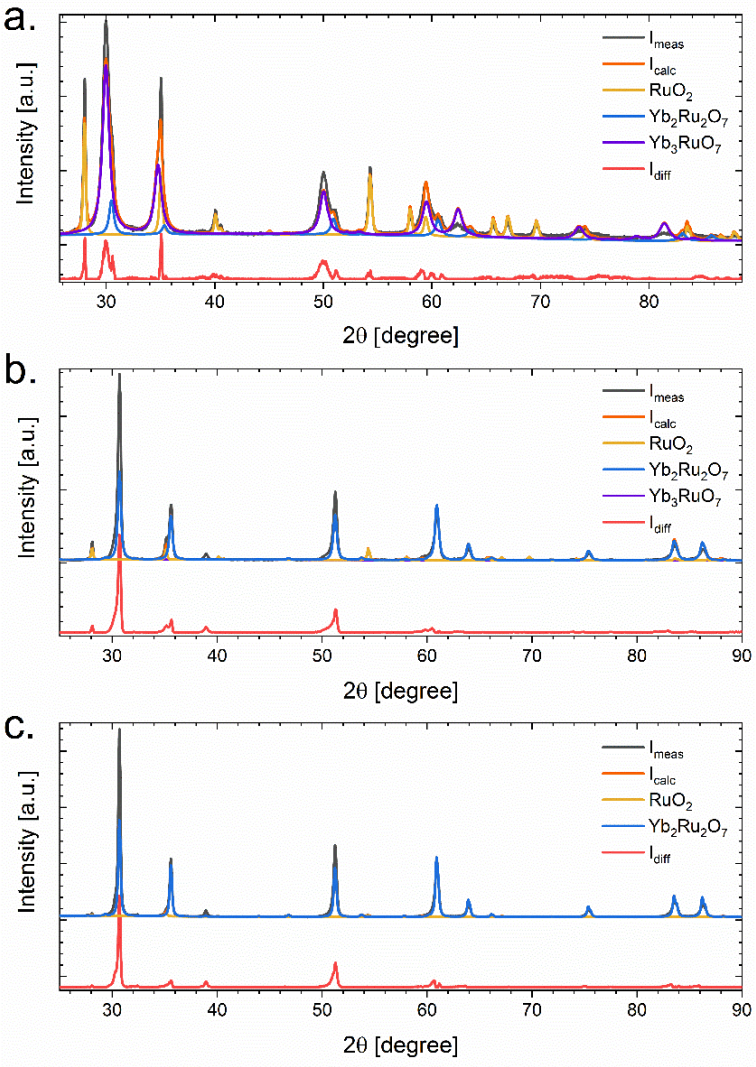

Figure S8. XRD pattern and Rietveld refinement results of the YbRu sample annealed at 800 °C for 4h (a), at 1020°C for 4h (b), and 1020°C for 24h (c).

Table S2. Composition, unit cell parameter of $Yb_2Ru_2O_7$, and quality of the fit of the full Rietveld refinement performed for the phase formation of the ytterbium ruthenium pyrochlore at different temperatures.

	at% RuO_2	**at.% Yb_3RuO_7**	**at.% $Yb_2Ru_2O_7$**	**a ($Yb_2Ru_2O_7$)/Å**	
650°C 4h	65.4	34.6	0	-	R_{wp}=11.69%, R_{exp}=4.39%, X^2=7.0909 GOF=2.6629
800°C 4h	53.1	31.5	15.4	10.124(13)	R_{wp}=14.69%, R_{exp}=4.39%, X^2=11.1973 GOF=3.3462
950°C 4h	18.0	46.2	35.8	10.083(2)	$_{wp}$=22.7%, R_{exp}=3.57%, X^2=40.4311 GOF=6.3585
1020°C 4h	11.4	4.0	84.6	10.085(1)	R_{wp}=27.33%, R_{exp}=3.84%, X^2=50.6544 GOF=7.1172
1020°C 24h	3.5	0	96.5	10.082(3)	R_{wp}=22.28%, R_{exp}=2.56%, X^2=75.7444 GOF=8.7031

Table S3 Composition of the prepared pyrochlore samples in atom % as obtained from the EDX analysis. The error is given as +/- one sigma in atom %.

	A-site, at%	B-site, at%	Oxygen, at%
$Yb_2Ru_2O_7$	18.1 (0.7)	17.1(1.0)	66.7 (2.7)
$Yb_2Ir_2O_7$	18.3(1.5)	17.9(1.2)	68.0 (4.3)
$Gd_2Ru_2O_7$	17.4(0.8)	16.3(0.5)	65.9(3.5)
$Gd_2Ir_2O_7$	19.0(1.9)	17.8(0.7)	64.1(4.3)
$Nd_2Ru_2O_7$	14.1(2.5)	15.3(1.8)	70.4(4.0)
$Nd_2Ir_2O_7$	12.4(0.9)	11.6(1.3)	70.9(4.5)

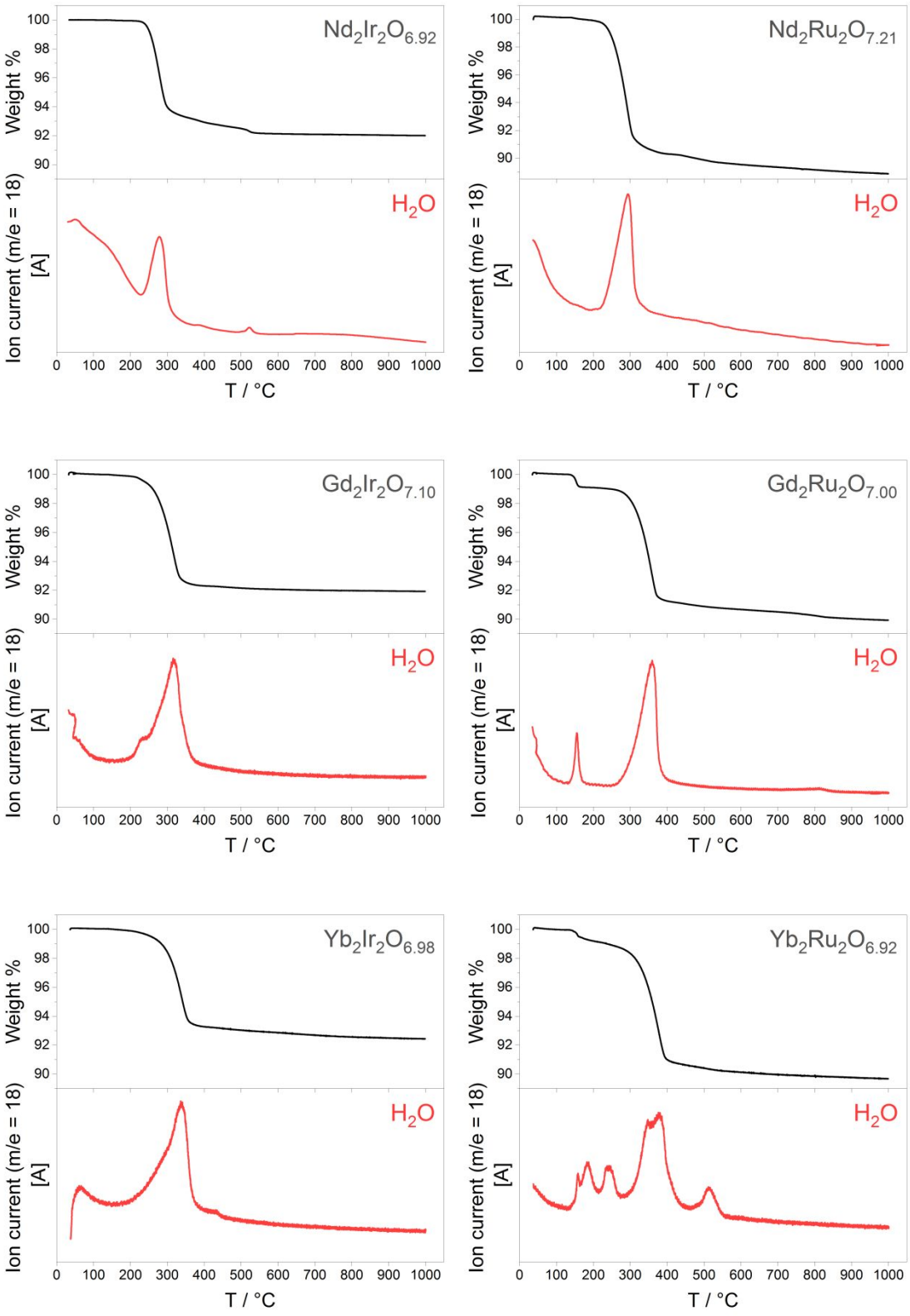

Figure S9. Thermogravimetric reduction analysis of the lanthanide pyrochlore materials used to quantify the oxygen stoichiometry and the related mass spectrometric signal tracking the water evolution with temperature. The actual oxygen stoichiometry for each pyrochlore is indicated in the chemical formula shown in each plot.

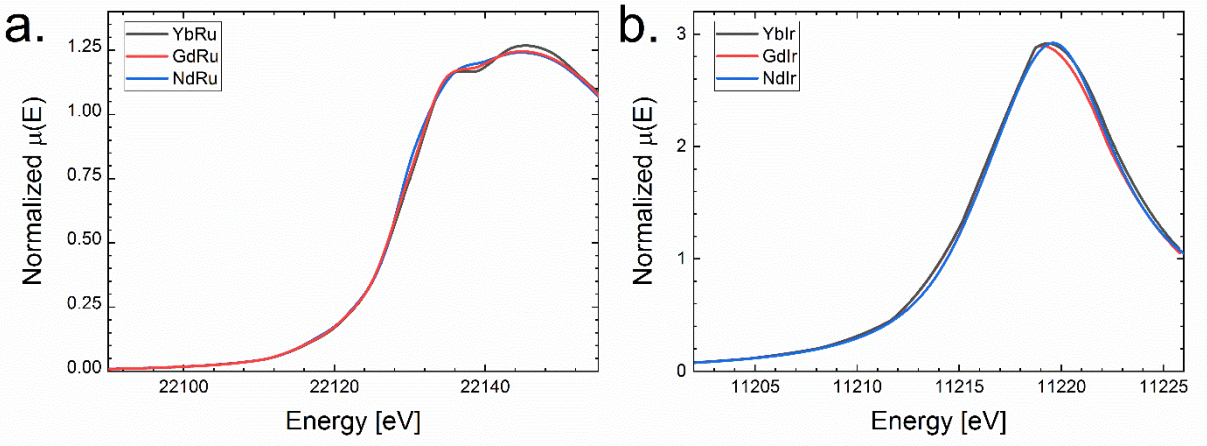

Figure S10. X-ray absorption near edge structure (XANES) spectra of the lanthanide pyrochlore materials at the Ru K-edge (a) and at the Ir L_{III} edge (b).